

An *RYR1* mutation associated with malignant hyperthermia is also associated with bleeding abnormalities

Rubén J. Lopez,¹ Susan Byrne,² Mirko Vukcevic,^{1,3} Marijana Sekulic-Jablanovic,¹ Lifan Xu,³ Marijke Brink,³ Jay Alamelu,⁴ Nicol Voermans,⁵ Marc Snoeck,⁶ Emma Clement,⁷ Francesco Muntoni,⁸ Haiyan Zhou,⁸ Aleksandar Radunovic,⁹ Shehla Mohammed,⁷ Elizabeth Wraige,² Francesco Zorzato,^{1,10*} Susan Treves,^{1,10*†} Heinz Jungbluth^{2,11,12*}

Malignant hyperthermia is a potentially fatal hypermetabolic disorder triggered by halogenated anesthetics and the myorelaxant succinylcholine in genetically predisposed individuals. About 50% of susceptible individuals carry dominant, gain-of-function mutations in *RYR1* [which encodes ryanodine receptor type 1 (RyR1)], though they have normal muscle function and no overt clinical symptoms. RyR1 is predominantly found in skeletal muscle but also at lower amounts in immune and smooth muscle cells, suggesting that *RYR1* mutations may have a wider range of effects than previously suspected. Mild bleeding abnormalities have been described in patients with malignant hyperthermia carrying gain-of-function *RYR1* mutations. We sought to determine the frequency and molecular basis for this symptom. We found that some patients with specific *RYR1* mutations had abnormally high bleeding scores, whereas their healthy relatives did not. Knock-in mice with the malignant hyperthermia susceptibility *RYR1* mutation Y522S (MHS *RYR1*_{Y522S}) had longer bleeding times than their wild-type littermates. Primary vascular smooth muscle cells from *RYR1*_{Y522S} knock-in mice exhibited a higher frequency of subplasmalemmal Ca²⁺ sparks, leading to a more negative resting membrane potential. The bleeding defect of *RYR1*_{Y522S} mice and of one patient was reversed by treatment with the *RYR1* antagonist dantrolene, and Ca²⁺ sparks in primary vascular smooth muscle cells from the MHS *RYR1*_{Y522S} mice were blocked by ryanodine or dantrolene. Thus, *RYR1* mutations may lead to prolonged bleeding by altering vascular smooth muscle cell function. The reversibility of the bleeding phenotype emphasizes the potential therapeutic value of dantrolene in the treatment of such bleeding disorders.

INTRODUCTION

Hemostasis is a stepwise process that causes bleeding to stop and can be grossly divided into primary and secondary hemostasis and three distinct stages. Primary hemostasis comprises (i) an instant vascular response to injury, leading to transient vasoconstriction limiting immediate blood loss, and (ii) platelet activation and aggregation, prompted by plasma von Willebrand factor (vWF) and sustained through platelet granule release that also enhances the initial vasoconstriction. Primary hemostasis results in for-

mation of a platelet plug aimed at provisionally stopping the bleeding. Secondary hemostasis involves (iii) the sequential activation of clotting factors present in the plasma in an inactive state through a cascade of reactions, ultimately leading to the formation of a fiber-like mesh called fibrin that surrounds the provisional platelet plug and causes definite blood coagulation (1).

Bleeding disorders are clinically and genetically heterogeneous and may affect all aspects of hemostasis. The most common causes are partial deficiencies of coagulation factors and fibrinolytic proteins, deficiencies in vWF, and platelet or connective tissue disorders (1). Nevertheless, mild bleeding disorders are common in the general population, but their precise incidence and their genetic background often remain unresolved (2, 3).

Mutations in *RYR1*, the gene encoding the skeletal muscle Ca²⁺ channel ryanodine receptor type 1 (RyR1), have a calculated frequency of 1:2000 to 1:3000 (4). Dominant *RYR1* mutations are commonly associated with malignant hyperthermia (MH), a severe pharmacogenetic reaction to halogenated anesthetics and muscle relaxants; exertional rhabdomyolysis/myalgia (ERM) (5); and the congenital myopathy central core disease (CCD). Recessive *RYR1* mutations have been associated with the congenital myopathies multi-minicore disease (MmD), centronuclear myopathy (CNM), and congenital fiber type disproportion (6–8). Bleeding abnormalities have been reported in isolated patients with MH susceptibility (MHS) (9–11), and homozygous mouse embryos knocked in for the MHS *RYR1* mutation Y522S (*RYR1*_{Y522S}) display massive edema and subcutaneous blood effusions at birth, suggestive of a severe bleeding disorder with antenatal onset (12).

Vascular smooth muscle cells play an important role in primary hemostasis, and changes in the intracellular Ca²⁺ concentrations play a central

¹Departments of Biomedicine and Anesthesia, Basel University Hospital, Hebelstrasse 20, 4031 Basel, Switzerland. ²Department of Paediatric Neurology, Neuromuscular Service, Evelina Children's Hospital, St Thomas' Hospital, London SE1 7EH, UK. ³Department of Biomedicine, Basel University Hospital, Hebelstrasse 20, 4031 Basel, Switzerland. ⁴Department of Haematology, Evelina Children's Hospital, St Thomas' Hospital, London SE1 7EH, UK. ⁵Department of Neurology, Radboud University Medical Centre, Nijmegen, Netherlands. ⁶National MH Investigation Unit, Department of Anesthesiology, Canisius Wilhelmina Hospital, 6532 Nijmegen, Netherlands. ⁷Department of Clinical Genetics, Guy's Hospital, London SE1 7EH, UK. ⁸Dubowitz Neuromuscular Centre, Institute of Child Health, University College London, London WC1N 1EH, UK. ⁹Department of Neurology, The Royal London Hospital, London E1 1BB, UK. ¹⁰Department of Life Sciences, General Pathology Section, University of Ferrara, Via Borsari 46, 44100 Ferrara, Italy. ¹¹Randall Division of Cell and Molecular Biophysics, Muscle Signalling Section, King's College, London SE1 1UL, UK. ¹²Department of Basic and Clinical Neuroscience, Institute of Psychiatry, Psychology & Neuroscience, King's College London, London SE5 9RX, UK.

*These authors contributed equally to this work.

†Corresponding author. Email: susan.treves@unibas.ch

mechanism regulating their relaxation and contraction (13). In addition to InsP_3 Rs, smooth muscle cells also express the three different RyR isoforms (13–17), and their Ca^{2+} homeostasis is more elaborate compared to many other excitable cell types. Whereas InsP_3 Rs act as channels releasing Ca^{2+} from the endo(sarco)plasmic reticulum leading to smooth muscle cell contraction, the specific role of RyRs is more complex, and in contrast to striated muscle, RyRs are involved in smooth muscle cell relaxation (13, 18, 19). We hypothesized that there may be a correlation between the presence of dominant MH-related *RYR1* mutations and mild bleeding abnormalities.

Here, we investigated the potential relationship between a mild bleeding disorder and the presence of dominant, gain-of-function *RYR1* mutations; we then used the heterozygous *RYR1*_{Y522S} mouse model to study the mechanism linking prolonged bleeding time to Ca^{2+} homeostasis in isolated smooth muscle cells. Our results indicated that gain-of-function *RYR1* mutations mainly affected Ca^{2+} homeostasis of smooth muscle cells by increasing “Spark” (spontaneous calcium release events) activity. We also demonstrated that administration of the specific RyR1 antagonist dantrolene, which is clinically approved for the treatment of MH reactions (20, 21), reversed the bleeding phenotype by decreasing spark activity in vascular smooth muscle cells.

RESULTS

Human subjects carrying *RYR1* mutations have a mild bleeding abnormality

To investigate bleeding in *RYR1*-associated myopathies, we invited *RYR1*-mutated individuals and their nonmutated relatives to complete a standardized questionnaire [molecular and clinical markers for the diagnosis and management of type 1 von Willebrand’s disease (MCMDM-1VWD)] validated for the evaluation of bleeding disorders (Table 1). Patients had neuromuscular features of MH, ERM, a congenital myopathy (CCD or MmD), or a combination of these features, associated mainly with dominant heterozygous *RYR1* missense mutations. A proportion of patients were compound heterozygous for two allelic *RYR1* mutations, reflecting that some *RYR1* mutations can be dominant with regard to MH but can be recessive with regard to the congenital myopathy phenotype. The neuromuscular features of patients from families 1, 2, 4, 6, 7, and 8 and of their relatives have been previously reported (5, 22, 23). MCMDM-1VWD bleeding questionnaires were obtained from 24 *RYR1*-mutated patients (12 females, 12 males) and 14 relatives without the familial *RYR1* mutation (4 females, 10 males). Symptoms of abnormal bleeding were common in *RYR1*-mutated individuals, characterized by severe menorrhagia and postpartum hemorrhage in females and milder symptoms of epistaxis and easy bruising in males. One male patient reported spontaneous hematomas in association with muscle cramps, whereas one female patient reported an additional history of recurrent and unexplained miscarriages. Improvement of menorrhagia was reported in one female (patient 4.2) after prescription of sodium dantrolene, the specific RyR1 antagonist used clinically to reverse acute MH reactions (20, 21), for her severe ERM. Baseline hematological studies including evaluation of clotting factors and platelet aggregation studies were normal in all patients with symptoms of increased bleeding, except in patients 2.6 and 2.7 in whom abnormal vWF levels were found, and patient 5.1 who had evidence of abnormal platelet function; bleeding scores from these patients were excluded from further statistical analysis because an alternative hematological diagnosis could not be confidently ruled out. Eight of 21 (38%) patients included in the statistical analysis had a pathological bleeding score (≥ 4) on the questionnaire compared to 0 of 14 (0%) of controls ($P = 0.0118$, two-tailed Fisher’s exact test). The mean bleeding score for patients is shown in Fig. 1A.

A mouse model knocked in for a human *RYR1* mutation associated with MHS shows prolonged bleeding times

To gain mechanistic insight linking *RYR1* mutations to bleeding, we used the heterozygous *RYR1*_{Y522S} MH-susceptible mouse (12). Applying a standardized test to accurately determine bleeding times in mice (24), we demonstrated that bleeding times in *RYR1*_{Y522S} mice were two to three times longer than in their wild-type littermates (Fig. 1B, bleeding times in male mice; fig. S1, bleeding times in female mice). Intraperitoneal dantrolene administration to wild-type mice before the bleeding test did not affect bleeding times. However, pretreatment of *RYR1*_{Y522S} mice with dantrolene, but not with vehicle alone, reduced bleeding to the same times as those seen in their wild-type littermates (Fig. 1B).

Bleeding times depend on the contraction of injured blood vessels, platelet number and function, and the activation of circulating clotting factors. We have previously not found a difference in the number and function of circulating platelets between wild-type and *RYR1*_{Y522S} mice (25). RyR1 is not detectable in platelets, virtually excluding disturbed platelet function as a potential cause for the bleeding disorder. Because wild-type and *RYR1*_{Y522S} knock-in littermates only differ in their *RYR1*, we hypothesized that these differences in bleeding times could be due to changes in the contraction and relaxation properties of the smooth muscle cells lining the blood vessels. Vessel reactivity can be assessed using a vessel injury model; however, because of their small size (with a diameter of 0.26 ± 0.03 mm), we could not accurately measure changes in the diameter of the tail artery, which would be a direct indication of contraction/relaxation. Furthermore, because of their predisposition to MH, deep anesthesia was not possible in the *RYR1*_{Y522S} knock-in mice, excluding the possibility of performing injury experiments in larger blood vessels. The fact that direct measurements could not be performed constitutes a limitation to our study. To demonstrate a cause-effect relationship between *RYR1* mutations and vessel response, we used the pulsed wave Doppler and measured velocity of blood flow (26, 27), at a point 1 cm upstream from the incision of the tail artery, at a constant blood pressure (fig. S2). Velocity of blood is inversely related to vessel diameter (28), and therefore, changes in velocity reflect changes in the contraction and relaxation status of smooth muscle cells. Under baseline conditions, there were no differences in blood flow velocity through the caudal artery between wild-type and *RYR1*_{Y522S} mice (Fig. 1C). However, in response to injury and more specifically at 8 to 10 min after incision, the velocity of blood flow in the tail artery of wild-type mice was significantly faster than in that of *RYR1*_{Y522S} mice. This result indirectly indicates that vasoconstriction occurs to a larger extent in the tail arteries of wild-type than in *RYR1*_{Y522S} mice.

Quantitative polymerase chain reaction (qPCR) experiments confirmed the expression of *RYR1* in primary arterial vascular smooth muscle cells, which was normalized to *DES*, which encodes desmin, a skeletal and smooth muscle cell-specific protein (29). Cells in mouse aorta and tail artery express the *RYR1* transcript, though as expected, to a much lower extent than skeletal muscle (Fig. 2A), and the presence of the *RYR1*_{Y522S} mutation in the heterozygous state does not affect the expression of *RYR1* (Fig. 2B) or of *RYR2* and *RYR3* (fig. S3). Reverse transcription PCR (RT-PCR) on mRNA isolated from tail arteries confirmed the expression of a mutated transcript in the heterozygous *RYR1*_{Y522S} mice (Fig. 2C). Confocal immunohistochemical analysis on isolated primary vascular smooth muscle cells confirmed the presence of the specific smooth muscle marker actin (Fig. 2D, central panels). Analysis of the subcellular distribution of RyR1 using an antibody that, under our experimental conditions, does not cross-react with RyR2 (fig. S4) showed that RyR1s are localized close to the plasma membrane (Fig. 2E, red). This distribution is similar to that of the voltage-sensing dihydropyridine receptor $\text{Ca}_v1.2$, which is found on the plasma membrane of vascular smooth muscle cells (Fig. 2E, green) (30–32).

Table 1. Genetic details, neuromuscular features, MCMDM-1VWD bleeding questionnaire scores, and bleeding phenotypes from patients with *RYR1*-related myopathies and their healthy relatives. Abnormal MCMDM-1VWD bleeding scores (≥ 4) are highlighted in red. Patient 1.1 was deceased, and the MCMDM-1VWD bleeding questionnaire was completed retrospectively on the basis of the information in the patient medical notes. Two dominant heterozygous MHS-related *RYR1* mutations were running independently in

families 5, 7, and 8. *RYR1*-mutated individuals in families 2 and 5 reported additional symptoms suggestive of smooth muscle involvement concerning both bladder and bowel (urinary incontinence, vesicoureteral reflux, and “spastic colon”). Neuromuscular features from families 1, 2, 4, 6, 7, and 8 have been previously reported. F, family; P/C, patient/control; S, sex; I, inheritance; NM, neuromuscular phenotype; *RYR1* +/-, *RYR1* mutation carrier state; BS, MCMDM-1VWD bleeding score; AR, autosomal recessive; AD, autosomal dominant.

| F | P/C | S | <i>RYR1</i> mutation(s) | I | NM | <i>RYR1</i> +/- | BS | Bleeding phenotype |
|---|------|---|------------------------------|----|----------|-----------------|----|--|
| 1 | 1.1 | F | p.R2241X, p.D708N; p.R2939K | AR | MmD/MH | + | 5 | Severe menorrhagia; postpartum bleeding |
| | 2.1 | F | p.G4638D | AD | CCD/MHS | + | 6 | Severe menorrhagia; postpartum bleeding |
| | 2.2 | F | p.G4638D | AD | CCD/MHS | + | 9 | Severe menorrhagia; postpartum bleeding |
| | 2.3 | M | — | — | — | — | -2 | Not applicable |
| | 2.4 | M | — | — | — | — | 3 | Rectal bleeding (diverticulitis ?); bleeding after dental extraction |
| 2 | 2.5 | M | — | — | — | — | 2 | Rectal bleeding (colitis ?) |
| | 2.6 | M | p.G4638D | AD | CCD/MHS | + | 4 | Epistaxis; easy bruising* |
| | 2.7 | M | p.G4638D | AD | CCD/MHS | + | 1 | Easy bruising* |
| | 2.8 | M | — | — | — | — | 0 | Not applicable |
| | 2.9 | F | — | — | — | — | -1 | Not applicable |
| | 2.10 | F | — | — | — | — | -2 | Not applicable |
| | 2.11 | M | — | — | — | — | -1 | Not applicable |
| 3 | 3.1 | F | p.S1342G, p.A1352G, p.T2787S | AD | ERM | + | 2 | Menorrhagia; epistaxis |
| | 3.2 | F | p.S1342G, p.A1352G, p.T2787S | AD | ERM | + | 2 | Menorrhagia; oral cavity bleeding |
| | 4.1 | F | p.G2434R | AD | ERM, MHS | + | 7 | Severe menorrhagia; epistaxis |
| | 4.2 | F | p.G2434R | AD | ERM, MHS | + | 4 | Severe menorrhagia [†] |
| 4 | 4.3 | M | — | — | — | — | 0 | Epistaxis |
| | 4.4 | F | — | — | — | — | -2 | Not applicable |
| | 4.5 | M | p.G2434R | AD | ERM, MHS | + | 3 | Epistaxis; bleeding after dental extraction |
| 5 | 5.1 | F | p.H3981Y | AD | ERM | + | 13 | Severe menorrhagia; postpartum bleeding* |
| | 5.2 | M | p.T4288_A4290dup; p.H3981Y | AD | ERM | + | 2 | Muscle hematoma after muscle cramps |
| | 6.1 | F | p.T4288_A4290dup | AD | ERM | + | 4 | Menorrhagia; postpartum bleeding |
| 6 | 6.2 | F | p.T4288_A4290dup | AD | ERM | + | 4 | Easy bruising; oral cavity bleeding; gastrointestinal bleeding |
| | 6.3 | M | p.T4288_A4290dup | AD | ERM | + | 1 | Bleeding from minor wounds |
| | 7.1 | M | p.V4849I | AD | ERM | + | -2 | Not applicable |
| 7 | 7.2 | M | p.V4849I | AD | ERM | + | -1 | Not applicable |
| | 7.3 | M | p.I2321V; p.V4849I | AD | ERM | + | 0 | Not applicable |
| | 7.4 | M | — | — | — | — | 0 | Not applicable |
| | 7.5 | F | — | — | — | — | 0 | Not applicable |
| | 7.6 | M | — | — | — | — | 0 | Not applicable |
| | 7.7 | M | — | — | — | — | 0 | Not applicable |
| | 8.1 | M | p.R614C | AD | MHS | + | 1 | Oral cavity bleeding |
| | 8.2 | M | p.R2676W | AD | MHS | + | -2 | Not applicable |
| 8 | 8.3 | M | p.R614C | AD | MHS | + | -1 | Not applicable |
| | 8.4 | M | — | — | — | — | -2 | Not applicable |
| | 8.5 | F | p.R2676W | AD | MHS | + | 2 | Menorrhagia |
| 9 | 9.1 | F | p.R2454H | AD | MHS | + | 4 | Easy bruising; postpartum bleeding; muscle hematoma |
| | 9.2 | M | p.R2454H | AD | MHS | + | -2 | Not applicable |

*Three patients (2.6, 2.7, and 5.1) were excluded from further statistical analysis because of abnormal vWF levels (2.6 and 2.7) and evidence of abnormal platelet function (5.1), respectively. [†]Patient 4.2 reported improvement of bleeding symptoms after commencement of dantrolene treatment, which was prescribed for exertional myalgia.

The subcellular distribution of RyR1 in isolated primary vascular smooth muscle cells is similar to that reported in pulmonary artery smooth muscle cells and in vas deferens (32–34); in the latter cells, localized RyR1-

mediated calcium release from subplasmalemmal stores causes activation of BK channels, resulting in cellular hyperpolarization, leading to vasodilation (34, 35).

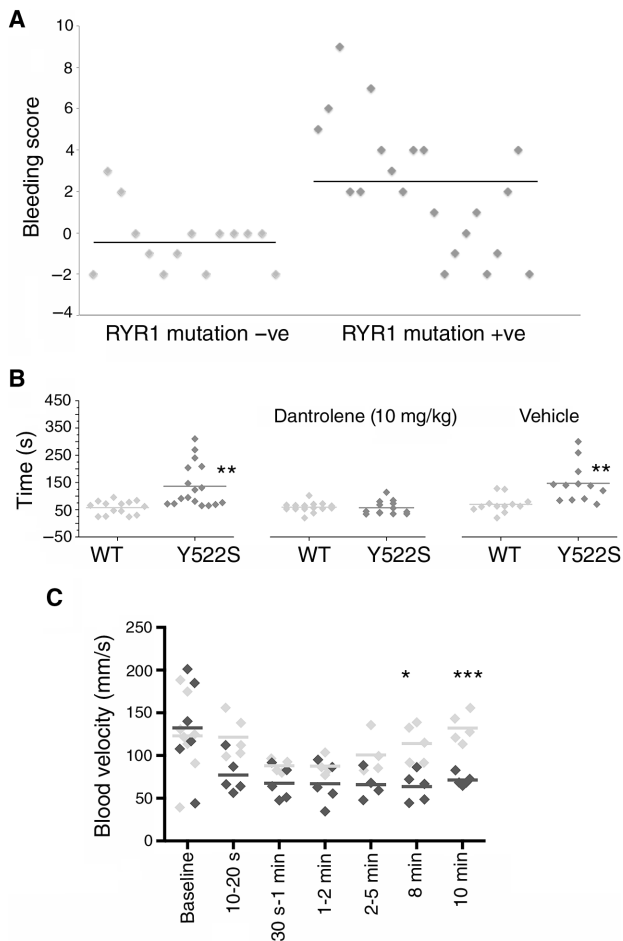


Fig. 1. *RYR1* mutations are associated with prolonged bleeding times. (A) Scatterplot of MCMDM-1VWD bleeding scores for *RYR1*-mutated patients compared to related controls without the familial *RYR1* mutation(s) (mean score of 2.3 in cases compared to -0.4 in controls; $P < 0.005$, Student's *t* test). Eight of 13 female patients had abnormal bleeding scores compared to 0 of 4 female controls ($P < 0.03$, Student's *t* test). The mean bleeding score for female patients was 4.5 (range, 2 to 9) and -1.3 (range, -2 to 0) in controls ($P < 0.0005$, Student's *t* test). (B) *RYR1*_{Y522S} knock-in MHS mice showed prolonged bleeding times that were reversed by dantrolene. Each symbol represents the bleeding time (in seconds) of a single wild-type (WT) (light gray) and *RYR1*_{Y522S} (dark gray) mouse. Mice were either untreated, pretreated with dantrolene, or pretreated with vehicle alone. ** $P < 0.05$, Student's *t* test. (C) Blood flow velocity in the caudal artery before and after incision. Each symbol represents the mean of five measurements performed on each mouse at the indicated time. Light gray symbols, WT mice; dark gray symbols, *RYR1*_{Y522S} mice. * $P < 0.004$ and *** $P < 0.0001$, Student's *t* test.

Calcium homeostasis in vascular smooth muscle cells isolated from the *RYR1*_{Y522S} mouse is significantly different compared to that of their wild-type littermates

To investigate how *RYR1* mutations affect Ca^{2+} homeostasis, we isolated primary vascular smooth muscle cells from mouse tail arteries. We used this cellular model, because bleeding times have been assessed on this tissue and

these cells are responsible for the control of the vasomotor activity in the tail (36). The resting Ca^{2+} concentration was similar in primary vascular smooth muscle cells isolated from wild-type and *RYR1*_{Y522S} mice (Fig. 3, A and B), though the latter cells showed significantly smaller total rapidly releasable Ca^{2+} stores compared to those isolated from wild-type littermates (Fig. 3C). In smooth muscle cells, local calcium release events termed " Ca^{2+} sparks" have been ascribed to the opening of single or clusters of RyR channels. Although they have little or no direct effect on contraction, they indirectly lead to vasodilation through activation of BK channels (13, 18). We studied spark activity in isolated primary vascular smooth muscle cells isolated from tail arteries loaded with the fast calcium dye Fluo-4. The frequency of calcium sparks is significantly higher in cells from the *RYR1*_{Y522S} mice than in those from their wild-type littermates (Fig. 3, D and E). Representative videos of sparks occurring in cells from wild-type and *RYR1*_{Y522S} mice are shown in videos S1 and S2, respectively. Detailed analysis of spark amplitude and kinetics revealed small but significant differences between cells isolated from wild-type and *RYR1*_{Y522S} knock-in mice (table S1).

We next used several drugs including RyR1 blockers and the $InsP_3$ R antagonist xestospongine C to determine the origin of these spontaneous Ca^{2+} release events. Sparks were extinguished in wild-type and *RYR1*_{Y522S} primary vascular smooth muscle cells by preincubation with ryanodine (Fig. 3E and video S3). Additionally, preincubation with dantrolene significantly decreased spark frequency in both wild-type and *RYR1*_{Y522S} cells (Fig. 3E and video S4). This effect was not observed when cells were incubated with the $InsP_3$ antagonist xestospongine C (video S5). These results indicated that RyR1 was present in primary vascular smooth muscle cells, that *RYR1* mutations leading to MHS were not only present in skeletal muscle but also in arterial smooth muscle cells, and that the *RYR1*_{Y522S} mutation increased the frequency of spark events. In skeletal muscle, *RYR1* mutations associated with MHS are gain-of-function mutations leading to an increased sensitivity to activating stimuli, resulting in prolonged and sustained muscle contractions (37–40). Our results suggested that a similar mechanism did not operate in smooth muscle cells, because *RYR1* mutations caused prolonged rather than shorter bleeding times, which would be expected if mutated RyR1 caused a gain of function in primary vascular smooth muscle cells. In skeletal muscle, excitation-contraction coupling depends on the mechanical interaction between the voltage-sensing dihydropyridine receptor and RyR1 (41), whereas in smooth muscle cells the functional unit is made up of dihydropyridine receptors, ryanodine receptors, and BK_{Ca} channels (13, 18). RyR-dependent Ca^{2+} sparks activate BK_{Ca} channels causing plasma membrane hyperpolarization, thereby decreasing Ca^{2+} influx through the dihydropyridine receptor and leading to smooth muscle relaxation (13, 18). We found that vascular smooth muscle cells from *RYR1*_{Y522S} mice were significantly more hyperpolarized than those from wild-type mice, which had membrane potentials in line with previous reports (Fig. 4A) (18). Furthermore, the membrane potential of cells from the *RYR1*_{Y522S} mice was reverted to control values after treatment with dantrolene (Fig. 4A).

DISCUSSION

Here, we demonstrate that gain-of-function *RYR1* mutations associated with MH and/or exertional rhabdomyolysis cause a mild but distinct bleeding disorder in humans and a corresponding phenotype in a murine model of MH, by affecting vascular smooth muscle cell calcium homeostasis. A model showing how *RYR1* mutations affect smooth muscle cell contraction is shown in Fig. 4B. Characteristic features of the human bleeding phenotype were female preponderance, presentation with marked menorrhagia, postpartum bleeding, and a history of miscarriages in the context of normal coagulation tests. Although in our study we evaluated

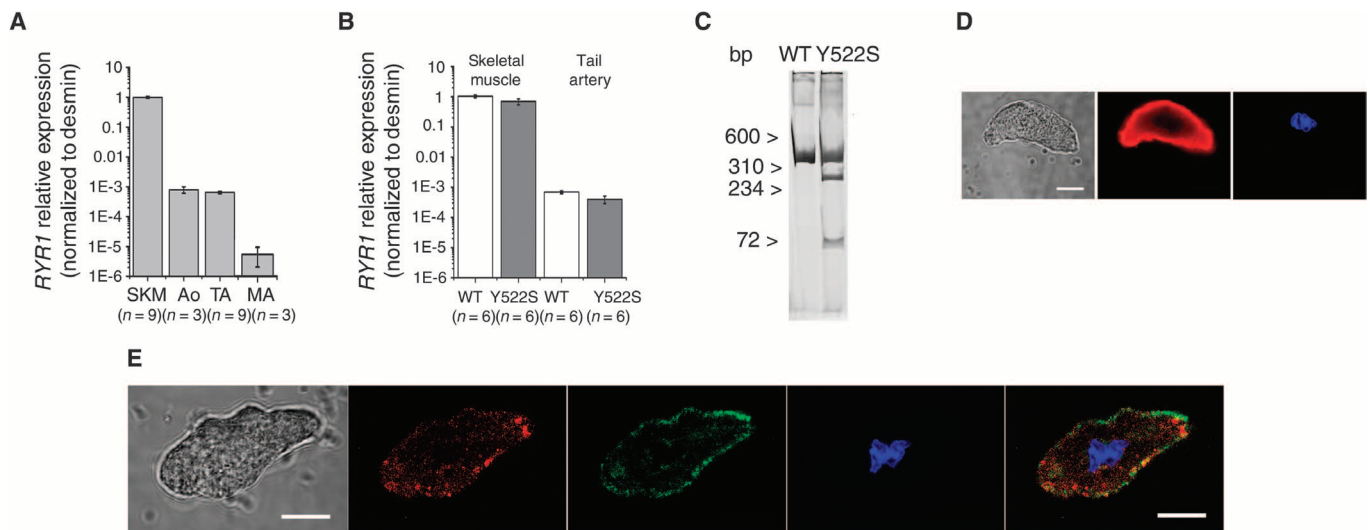


Fig. 2. RyR1 is present at the mRNA and protein level in aortae and tail arteries and is localized close to the plasma membrane. **(A)** *RYR1* expression in skeletal muscle (SKM), aorta (Ao), tail (TA), and mesenteric artery (Ma) was normalized to *DES* content, which is present in skeletal and smooth muscle cells (29). The numbers below the bars indicate number of mice used for the analysis. **(B)** The presence of the Y522S mutation does not affect *RYR1* expression as determined by qPCR. The numbers below the bars indicate number of mice used for the analysis. **(C)** Total RNA was extracted from purified aortas, and the expression of *RYR1* was evaluated by RT-PCR. Digestion of the amplified *RYR1* cDNA (complementary DNA) from WT mice yielded the uncut band of about 376 base pairs (bp). Digestion of the cDNA from heterozygous *RYR1*_{Y522S} mice yielded two bands of 276 and 100 bp plus the uncut 376-bp band from the WT allele. Image is

representative of two independent experiments, with two mice analyzed per genotype. **(D)** Phase contrast of an isolated primary vascular smooth muscle cell (left); confocal immunofluorescence on the same cell using a mouse antibody specific for smooth muscle actin followed by anti-mouse Alexa Fluor 569 (middle) or DAPI (4',6-diamidino-2-phenylindole) to localize the nucleus (right). Images are representative of cells from four mice per genotype. **(E)** Phase contrast on an isolated primary vascular smooth muscle cell (leftmost image). Confocal immunofluorescence of the same cell stained with mouse monoclonal anti-RyR1 antibody followed by anti-mouse Alexa Fluor 568 (red), rabbit anti-Ca_v1.2 followed by anti-rabbit Alexa Fluor 488 (green), and DAPI (blue). Composite image showing colocalization of RyR1 and Ca_v1.2 (rightmost image). Images are representative of cells from four mice per genotype. Scale bars, 10 μm.

a relatively small sample of *RYR1*-mutated patients and controls, the clinical data are consistent with the data obtained from the corresponding mouse model carrying the murine equivalent of a human MH-related *RYR1* mutation (12). The large variation in the bleeding times of *RYR1*_{Y522S} mice may reflect different extents of contraction of the skeletal muscles within the mouse tail when placed at 37°C. Alternatively, it may be due to intrinsic structural properties of the tetrameric RyR1 complex, which may or may not contain RyR1 mutants. A variation in the proportion of protomers encoded by wild-type and mutated alleles within the tetrameric RyR1 Ca²⁺ channel complex affects the biophysical properties of the RyR1 complex (42) and therefore may account for the variability of the calcium signals responsible for vascular responses. This explanation agrees with the data obtained from wild-type mice, which exhibit much more consistent bleeding times, presumably because of the homogeneous protomeric composition within the RyR1 tetrameric protein complex. Our mouse data are also consistent with our findings from humans, in that higher mean bleeding scores correlated with greater variability in *RYR1*-mutated patients compared to relatives without the familial *RYR1* mutation. Prolonged bleeding times in the *RYR1*_{Y522S} mice and in one patient were reversed by administration of the specific RyR1 antagonist dantrolene, supporting an association between the observed bleeding phenotype and the *RYR1* mutant state. These results suggest that dantrolene could be administered as a pharmacological treatment for *RYR1*-related bleeding disorders and, potentially, other causes of prolonged bleeding due to impaired vascular smooth muscle cell contractility

rather than primary platelet or coagulation factor abnormalities. Considering that carriers of MH-associated *RYR1* mutations are frequent (1:2000 to 1:3000) (4) but often asymptomatic unless exposed to triggering agents, such mutations may account for common mild bleeding abnormalities in humans that are currently without genetic explanation. Notably, we found evidence of abnormal platelet function and borderline reduced vWF levels in one and two *RYR1*-mutated patients within our cohort, respectively. These patients were not considered for the final statistical analysis, because we could not exclude a primary platelet or vWF abnormality as an alternative explanation for the observed bleeding phenotype. However, similar findings of mildly abnormal platelet function and vWF levels have been reported in other nonhematological disorders associated with prolonged bleeding such as collagen disorders (43) or Noonan syndrome (44), where the primary defect does not concern platelets or coagulation factors and may therefore well be a secondary feature also in the *RYR1*-related bleeding disorder reported in this study.

Our observations are consistent with emerging knowledge concerning the dynamic and complex role of BK_{Ca} channels and RyR in tissue-specific vasoregulation. Pressure-induced RyR activation in mesenteric resistance arteries has a strong vasodilatory effect, mediated by Ca²⁺-induced activation of BK_{Ca} channels and, possibly, Ca²⁺-induced inactivation of L-type voltage-dependent Ca²⁺ channels (45). Considering that RyR2 rather than RyR1 is the predominant RyR isoform in murine mesenteric arteries (17), the *RYR1*-associated arterial smooth muscle cell phenotype seems unexpected.

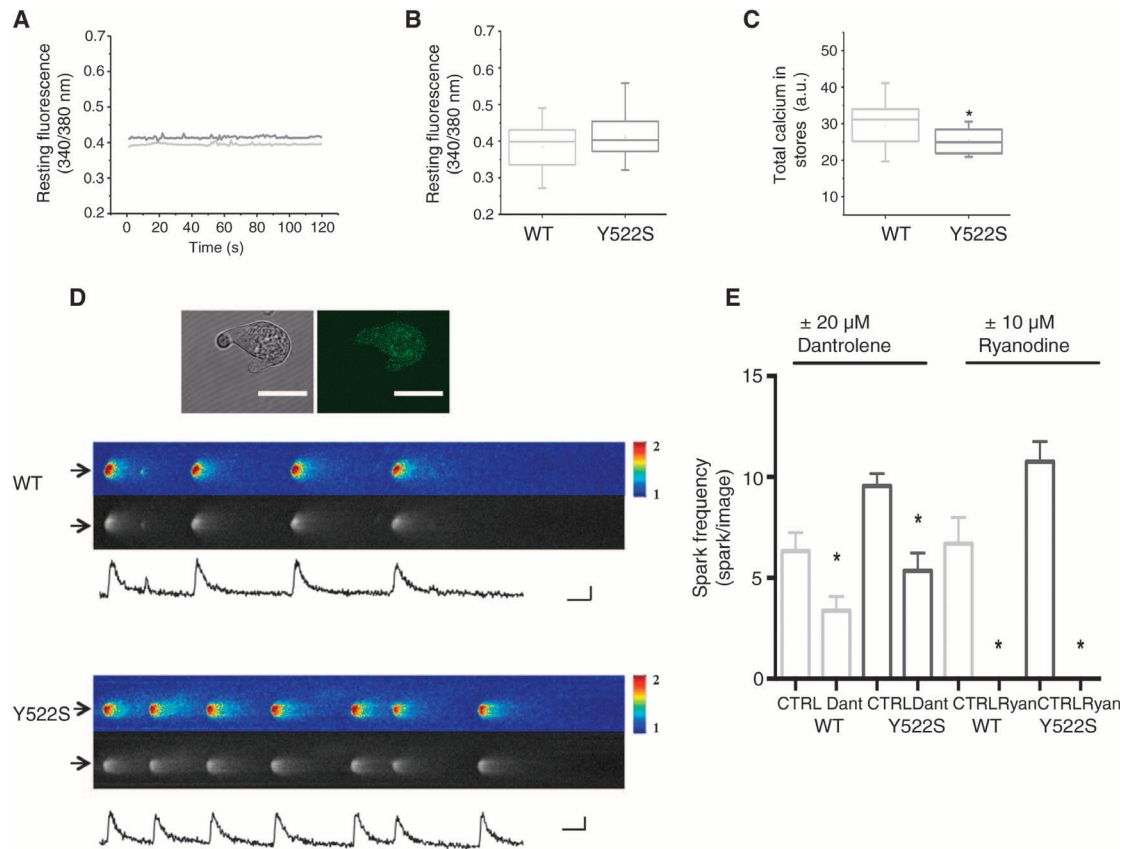


Fig. 3. Arterial smooth muscle cells from $RYR1_{Y522S}$ mice exhibit smaller intracellular Ca^{2+} stores and a higher frequency of spontaneous Ca^{2+} sparks. (A) Representative Fura-2 traces of resting fluorescence ratios (340/380 nm) of primary vascular smooth muscle cells isolated from WT (light gray) and $RYR1_{Y522S}$ (dark gray) mice. (B) Mean resting fluorescence ratios from primary vascular smooth muscle cells isolated from two WT ($n = 20$ cells) and two $RYR1_{Y522S}$ knock-in ($n = 20$ cells) mice. The values were not significantly different. (C) Total amount of Ca^{2+} in the thapsigargin/ionomycin-sensitive stores was significantly lower in vascular smooth muscle cells from two $RYR1_{Y522S}$ mice ($n = 20$ cells) compared to those from two WT ($n = 20$ cells) mice. $*P < 0.05$, Student's t test. a.u., arbitrary units. (D) Top row: Bright-field image (left) and Fluo-4 fluorescent photomicrograph (right) of an isolated smooth muscle cell. Scale bars, 10 μ m. Bottom rows: Representative pseudocolor and grayscale linescan images of spontaneous localized calcium release events (sparks) in vascular smooth muscle cells. Experiments were performed on cells from WT (top) and $RYR1_{Y522S}$ (bottom) mice. The color scale indicates the fluorescence change calculated as the FF_0 ratio. The traces under the linescan images show the time course of the calcium sparks. Scale bars, 10 μ m (vertical); 100 ms (horizontal); pseudocolor FF_0 . (E) Mean (\pm SEM) spark frequency in vascular smooth muscle cells from six WT (light gray, $n = 28$ cells) and six $RYR1_{Y522S}$ (dark gray, $n = 28$) mice, treated as indicated with dantrolene (Dant). $**P < 0.03$, $***P < 0.0001$, Student's t test when comparing cells \pm dantrolene and \pm ryanodine (Ryan).

However, in this context, a distinct spatial distribution may be more important than a relative amount of RyR isoforms. As we have demonstrated in murine arterial smooth muscle cells, RyR1s are predominantly found subsarcolemmally, and altered activity of the mutant RyR1s may be more consequential because of their close proximity to BK_{Ca} channels. We also cannot exclude the possibility that the release of Ca^{2+} from mutated RyR1 channels may facilitate the opening of adjacent RyR2 channels through the regenerative Ca^{2+} -induced Ca^{2+} release mechanism (46).

Our study reports a nonneuromuscular phenotype, that is, abnormal bleeding, in $RYR1$ -related myopathies and is likely to inform the surveillance and anticipatory management of patients affected by these conditions. Considering that RyR1 is found in many types of tissues, nonneuromuscular manifestations of $RYR1$ mutations are not unexpected but may have been overlooked, because they are mild and/or involve

symptoms that are not necessarily considered part of a neuromuscular disorder. The marked female preponderance in our series with severe menorrhagia and/or postpartum hemorrhage raises the question of more extensive smooth muscle cell involvement in $RYR1$ -related myopathies. This additional smooth muscle cell involvement may confound the observed bleeding phenotype, in a gender-specific manner in particular on the uterine level, considering that smooth muscle cells also play an important role in uterine vasoregulation and myometrial contraction (47, 48). Patients from two of our families reported prominent bowel and bladder involvement (urinary incontinence, vesicoureteral reflux, and spastic colon), suggesting a more widespread smooth muscle cell involvement, also in keeping with a role of both RyRs and BK_{Ca} channels in bladder smooth muscle signaling (49). Although it is beyond the goal of the present study to specifically investigate bleeding abnormalities in patients with $RYR1$ mutations, these observations should prompt future investigations into

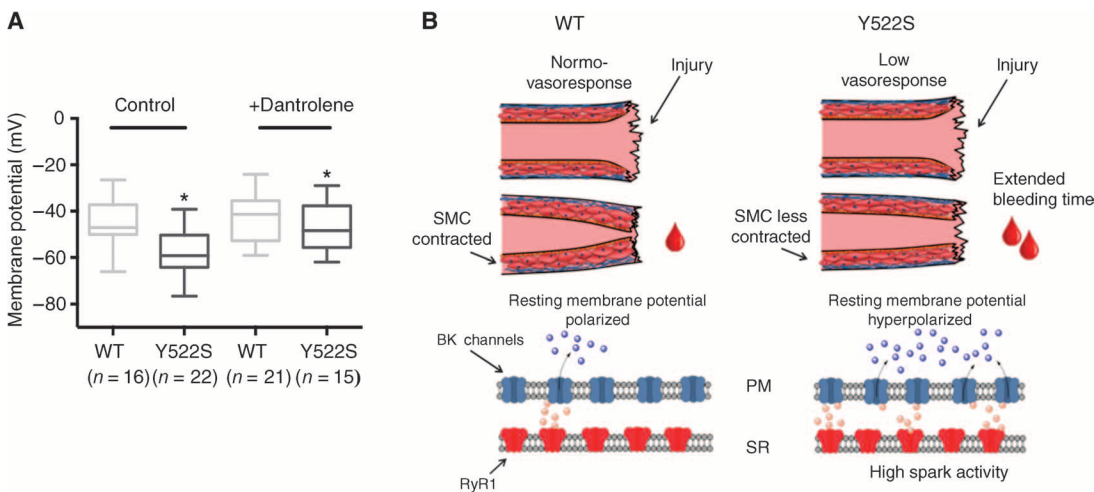


Fig. 4. Smooth muscle cells from *RYR1*_{Y522S} mice are more hyperpolarized than those from WT mice, and schematic representation of RyR1 function in arterial smooth muscle cells. (A) The resting membrane potential was measured using the potentiometric probe bis-oxonol in vascular smooth muscle cells from WT mice (seven controls, two +dantrolene) and *RYR1*_{Y522S} mice (four controls and two +dantrolene) (see also fig. S5). *n* indicates the number of individual cells that were assessed. Cells were either left untreated (control) or pretreated with 20 μ M dantrolene for 30 min. **P* < 0.05, Student's *t* test, mean resting membrane potential was significantly different between WT and *RYR1*_{Y522S} mice. **(B)** Schematic representation of the mechanism leading to prolonged bleeding time due to *RYR1* mutations. In normal conditions (left panel), early vasospasm occurring immediately after injury reduces bleeding (in coordination with platelets and coagulation factors not shown here). Mutations in *RYR1* (right panel) result in hyperpolarization of the smooth muscle cell (SMC) membrane potential, reducing the ability of vessels to contract and ultimately increasing the bleeding time. PM, plasma membrane; SR, sarcoplasmic reticulum; BK, calcium-activated potassium channel. Blue balls, potassium; peach balls, calcium sparks; RyR1_{Y522S}, MH knock-in.

the association between *RYR1* mutations and a more generalized smooth muscle dysfunction on both the clinical and the cellular level.

MATERIALS AND METHODS

Patients

Patients were identified through the participating tertiary neuromuscular and MH centers. Genetic testing and hematological studies including evaluation of clotting factors and platelet aggregation were performed as part of the routine diagnostic workup. Patients were invited to complete the MCMDM-1VWD bleeding questionnaire, a validated and widely used diagnostic tool in the evaluation of bleeding disorders (50). MCMDM-1VWD bleeding questionnaires were scored independently by two clinicians blinded to the genetic status (mutated or nonmutated) of the proband. The study received UK Research Ethics Committee approval (15/WS/204, granted by the West of Scotland REC 5). Patients gave informed consent for anonymized publication of their clinical information.

Animal model

Experiments were carried out on 7- to 12-week-old heterozygous *RYR1*_{Y522S} knock-in mice and their wild-type littermates. The mouse model was generated by Chelu *et al.* (12) and was a gift from S. Hamilton (Baylor College of Medicine, Houston, TX). Experimental procedures were approved by the Veterinary Cantonal Authorities (permit numbers 1728 and 1729).

Bleeding time assay

Bleeding time was determined according to Liu *et al.* (24). Intraperitoneal injections with dantrolene (10 mg/kg) or vehicle alone (saline solution) were administered 1 hour before bleeding time determination.

Pulsed wave Doppler
Male mice (15 to 20 weeks old) were lightly anesthetized with ketamine/xylazine [ketamine (95 mg/kg) + xylazine (10 mg/kg)] and placed on a heated blanket at 26°C. Blood flow velocity in the tail artery was measured using a pulsed wave Doppler ultrasound system (Vevo 2100, VisualSonics Inc.) at high frequency (32 MHz, MS-550D transducer). The probe was positioned where a consistent signal could be detected at the proximal end of the tail, about 1 cm from the base of the tail. Velocity of blood flow was measured before and at 6 time points after an incision was made on the tail artery; measurements were made 1 cm upstream from the incision site. The velocity was measured during five consecutive cardiac cycles, and the mean blood flow velocity per mouse was plotted at each time point before and after

incision. The experimenters were blinded and had no previous knowledge of the genotype of the mice. Data were analyzed and plotted using the GraphPad Prism V 6.0 and OriginPro 8.6.0 softwares.

Blood pressure measurements

Systolic blood pressure was monitored in conscious mice using a non-invasive tail-cuff photoplethysmography system (BP-2000 Blood Pressure Analysis System, Visitech Systems). Blood pressures were assessed in a quiet environment at the same time of day, for a period of 7 days before the actual measurements, to allow the mice to adjust to the protocol. Each symbol represents the blood pressure value of individual mice.

Isolation of single smooth muscle cells

Primary vascular smooth muscle cells were isolated essentially as described (51) using an enzymatic cocktail containing papain (9.6 U/ml) (Sigma, #P4762), collagenase (1200 U/ml) (Worthington, #LS004176), elastase (2.58 U/ml) (Worthington, #LS002292), 0.6% bovine serum albumin, and soybean trypsin inhibitor (1 mg/ml) (Worthington, #LS003587).

Calcium imaging and Spark analysis

The resting calcium fluorescence was measured using the calcium indicator Fura-2 AM (Invitrogen) (25), and the total amount of Ca²⁺ present in the rapidly releasable intracellular stores was determined as previously described (52). Calcium sparks were measured in cells loaded with 5 μ M Fluo-4 using a Nikon A1R laser-scanning confocal microscope (Nikon Instruments Inc.) with a 60 \times oil immersion Plan Apo VC Nikon objective (numerical aperture, 1.4). Five-second-duration linescan images (*x,t*) were acquired in resonant mode at super high temporal resolution (7680 fps) with 512 pixels (0.05 μ m/pixel) in the *x* direction and 39936 pixels (0.126 ms/pixel) in the *t* direction using a pinhole size of 72.27 μ m. Four

to five images were taken at different positions across each cell. Fluo-4 was excited with a laser at 487 nm, and the fluorescence emitted at 525 ± 25 nm was recorded. Images were analyzed using the open-source image processor software Fiji (53). After binning $4\times$ in the temporal axes, linescan images were run with the automated sparks processor plug-in SparkMaster (54).

Immunofluorescence

Cells were fixed with ice-cold methanol/acetone (1:1) for 30 min and processed as previously described (52). The primary antibodies used were mouse anti-smooth muscle actin (Sigma, #A5228), mouse anti-RyR1 (Thermo Scientific, #MA3-925), and rabbit anti- $\text{Ca}_v1.2$ (Santa Cruz Biotechnology, #sc-25686). The secondary conjugates were anti-mouse Alexa Fluor 568 and chicken anti-rabbit Alexa Fluor 488 (LuBioScience). Nuclei were counterstained with DAPI (25 to 30 μM) for 5 min before mounting. Cells were examined by confocal microscopy using a Nikon A1R laser-scanning confocal microscope with a $60\times$ oil immersion Plan Apo objective.

Real-time qPCR and RT-PCR

Total RNA was extracted and treated with deoxyribonuclease I (Invitrogen) as previously described (25). After RT using 1000 to 1500 ng of RNA, cDNA was amplified by real-time qPCR with a 7500 Fast Real-Time PCR system (Applied Biosystems) using SYBR Green technology (Fast SYBR Green Master Mix, Applied Biosystems) and the following primers: *RYR1*, 5'-TCACTCACAATGGAAAGCAG-3' (forward) and 5'-AGCAGAATGACGATAACGAA-3' (reverse); *DES*, 5'-TGAGACCATCGCGGCTAAGA-3' (forward) and 5'-GTGTCCGTTATCCATCATCTCC-3' (reverse). Gene expression was normalized to desmin (*DES*) content, because this marker is specifically expressed in muscle cells (29, 55). *RYR1* expression levels in mouse aorta, tail artery, and mesenteric artery were compared to *RYR1* expression levels in extensor digitorum longus, that latter being the reference tissue set to 1. *RYR1* expression in aorta was also investigated by semiquantitative RT-PCR as previously described (25).

Membrane potential measurements

Membrane potential measurements were performed using the potentiometric fluorescence dye bis-oxonol as described (56). Briefly, isolated arterial smooth muscle cells were plated on laminin/gelatin (1:10 ratio) precoated coverslips and allowed to attach for 20 min in a modified Krebs-Ringer solution (140 mM NaCl, 0.5 mM CaCl_2 , 5 mM KCl, 1 mM MgSO_4 , 10 mM Hepes, 1 mM Na_2HPO_4 , 5.5 mM glucose, and 1% albumin). Cells were loaded with the potentiometric fluorescence dye bis-oxonol (Molecular Probes, #B438) in the presence or absence of 20 μM dantrolene at room temperature for 30 to 40 min. To calibrate the membrane potential cells were incubated with the Na^+ ionophore gramicidin (10 μM) (Sigma, #G-5002) and then exposed to different Na^+ -containing solutions (fig. S5). The concentration ratios of Na^+ and choline were varied to maintain $[\text{Na}^+] + [\text{choline}] = 144$ mM. Theoretical values for membrane potential were calculated according to the formula $E_m = 60 \log([\text{Na}^+]_o + [\text{K}^+]_o) / ([\text{Na}^+]_i + [\text{K}^+]_i)$ and considering the internal concentration of Na^+ and K^+ as described by Nelson *et al.* (18). Fluorescence was recorded every 0.5 min with a Nikon A1+ confocal microscope, using a $60\times$ oil objective. Samples were illuminated with a sapphire laser at 488 nm, and the fluorescence emitted at 525/50 nm was recorded. Fluorescence images were processed using the open-source software Fiji.

Statistical analysis and graphical software

Statistical analysis on the MCMDM-1VWD bleeding questionnaires was performed by converting raw bleeding scores to binary numbers for use in Fisher's exact test with two-tailed *P* value (negative screening test ≤ 3 , positive screening test ≥ 4). Mean scores were compared using Student's *t* test.

For all other experiments, statistical analysis was performed using the Student's *t* test; means were considered statistically significant when the *P* value was <0.05 . Data were processed, analyzed, and plotted using the software OriginPro 8.6.0 (OriginLab Corporation). Images were assembled using Adobe Photoshop CS (version 8.0).

SUPPLEMENTARY MATERIALS

www.sciencesignaling.org/cgi/content/full/9/435/ra68/DC1

Fig. S1. *RYR1*_{Y522S} female mice also exhibit prolonged bleeding times.

Fig. S2. Heart rate and systolic blood pressure are similar in wild-type and *RYR1*_{Y522S} mice.

Fig. S3. Expression of *RYR2* and *RYR3* is not significantly different in the tail arteries of wild-type and *RYR1*_{Y522S} mice.

Fig. S4. Specificity of the anti-RyR1 antibodies used for immunohistochemistry.

Fig. S5. Membrane potential measurements using the fluorescence potentiometric probe bis-oxonol.

Table S1. Detailed analysis of full kinetic parameters of sparks in vascular smooth muscle cells from wild-type and *RYR1*_{Y522S} mice.

Video S1. Sparks in smooth muscle cells from wild-type mice.

Video S2. Sparks in smooth muscle cells from *RYR1*_{Y522S} mice.

Video S3. Sparks in smooth muscle cells from wild-type mice after treatment with 10 μM ryanodine.

Video S4. Sparks in smooth muscle cells from *RYR1*_{Y522S} mice after treatment with 20 μM dantrolene.

Video S5. Sparks in smooth muscle cells from *RYR1*_{Y522S} mice after treatment with 250 nM xestospongine C.

REFERENCES AND NOTES

1. D. L. Kasper, *Harrison's Principles of Internal Medicine*, D. L. Kasper, A. Fauci, S. L. Hauser, D. L. Longo, J. L. Jameson, J. Loscalzo, Eds. (McGraw Hill Education Medical, New York, ed. 19, 2015).
2. A. Tosetto, G. Castaman, F. Rodeghiero, Bleeders, bleeding rates, and bleeding score. *J. Thromb. Haemost.* **11** (Suppl. 1), 142–150 (2013).
3. P. H. Shaw, S. Reynolds, S. Gunawardena, L. Krishnamurti, A. K. Ritchey, The prevalence of bleeding disorders among healthy pediatric patients with abnormal pre-procedural coagulation studies. *J. Pediatr. Hematol. Oncol.* **30**, 135–141 (2008).
4. N. Monnier, R. Krivosic-Horber, J.-F. Payen, G. Kozak-Ribbens, Y. Nivoche, P. Adnet, H. Reyford, J. Lunardi, Presence of two different genetic traits in malignant hyperthermia families: Implication for genetic analysis, diagnosis, and incidence of malignant hyperthermia susceptibility. *Anesthesiology* **97**, 1067–1074 (2002).
5. N. Dlamini, N. C. Voermans, S. Lillis, K. Stewart, E.-J. Kamstee, G. Drost, R. Quinlivan, M. Snoeck, F. Norwood, A. Radonovic, V. Straub, M. Roberts, A. E. Vrancken, W. L. van der Pol, R. I. F. M. de Coov, A. Y. Manzur, S. Abbs, A. King, M. Lammens, P. M. Hopkins, S. Mohammed, S. Treves, F. Muntoni, E. Wraige, M. R. Davis, B. van Engelen, H. Jungbluth, Mutations in *RYR1* are a common cause of exertional myalgia and rhabdomyolysis. *Neuromuscul. Disord.* **23**, 540–548 (2013).
6. S. Treves, H. Jungbluth, F. Muntoni, F. Zorzato, Congenital muscle disorders with cores: The ryanodine receptor calcium channel paradigm. *Curr. Opin. Pharmacol.* **8**, 319–326 (2008).
7. I. Colombo, M. Scoto, S. A. Robb, L. Maggi, V. Gowda, T. Cullup, M. Yau, R. Phadke, C. Sewry, H. Jungbluth, F. Muntoni, Congenital myopathies: Natural history of a large pediatric cohort. *Neurology* **84**, 28–35 (2015).
8. M. Denborough, Malignant Hyperthermia. *Lancet* **352**, 1131–1135 (1998).
9. C. R. Stephen, Fulminant hyperthermia during anesthesia and surgery. *JAMA* **202**, 178–182 (1967).
10. W. G. Cullen, Malignant hyperpyrexia during general anaesthesia: A report of two cases. *Can. Anaesth. Soc. J.* **13**, 437–443 (1966).
11. J. C. Daniels, I. M. Polayes, R. Villar, F. W. Hehre, Malignant hyperthermia with disseminated intravascular coagulation during general anesthesia: A case report. *Anesth. Analg.* **48**, 877–883 (1969).
12. M. Chelu, S. A. Goonasekera, W. J. Durham, W. Tang, J. D. Lueck, J. Riehl, I. N. Pessah, P. Zhang, M. B. Bhattacharjee, R. T. Dirksen, S. L. Hamilton, Heat- and anesthesia-induced malignant hyperthermia in an RyR1 knock-in mouse. *FASEB J.* **20**, 329–330 (2006).
13. M. J. Berridge, Smooth muscle cell calcium activation mechanisms. *J. Physiol.* **586**, 5047–5061 (2008).
14. Y.-M. Zheng, Q.-S. Wang, Q.-H. Liu, R. Rathore, V. Yadav, Y.-X. Wang, Heterogeneous gene expression and functional activity of ryanodine receptors in resistance and conduit pulmonary as well as mesenteric artery smooth muscle cells. *J. Vasc. Res.* **45**, 469–479 (2008).
15. T. Vaithianathan, D. Narayanan, M. T. Asuncion-Chin, L. H. Jeyakumar, J. Liu, S. Fleischer, J. H. Jaggard, A. M. Dopico, Subtype identification and functional characterization of ryanodine receptors in rat cerebral artery myocytes. *Am. J. Physiol. Cell Physiol.* **299**, C264–C278 (2010).

16. X.-Q. Li, Y.-M. Zheng, R. Rathore, J. Ma, H. Takeshima, Y.-X. Wang, Genetic evidence for functional role of ryanodine receptor 1 in pulmonary artery smooth muscle cells. *Pflugers Arch.* **457**, 771–783 (2009).
17. E. B. Westcott, E. L. Goodwin, S. S. Segal, W. F. Jackson, Function and expression of ryanodine receptors and inositol 1,4,5-trisphosphate receptors in smooth muscle cells of murine feed arteries and arterioles. *J. Physiol.* **590**, 1849–1869 (2012).
18. M. T. Nelson, H. Cheng, M. Rubart, L. F. Santana, A. D. Bonev, H. J. Knot, W. J. Lederer, Relaxation of arterial smooth muscle by calcium sparks. *Science* **270**, 633–637 (1995).
19. J. H. Jaggard, V. A. Porter, W. J. Lederer, M. T. Nelson, Calcium sparks in smooth muscle. *Am. J. Physiol. Cell Physiol.* **278**, C235–C256 (2000).
20. T. Krause, M. U. Gerbershagen, M. Fiege, R. Weijthorn, F. Wappler, Dantrolene—A review of its pharmacology, therapeutic use and new developments. *Anaesthesia* **59**, 364–373 (2004).
21. B. R. Fruen, J. R. Mickelson, C. F. Louis, Dantrolene inhibition of sarcoplasmic reticulum Ca^{2+} release by direct and specific action at skeletal muscle ryanodine receptors. *J. Biol. Chem.* **272**, 26965–26971 (1997).
22. M. Snoeck, B. G. van Engelen, B. Kusters, M. Lammens, R. Meijer, J. P. F. Molenaar, J. Raaphorst, C. C. Verschuuren-Bemelmans, C. S. M. Straathof, L. T. L. Sie, I. F. de Co, W. L. van der Pol, M. de Visser, H. Scheffer, S. Treves, H. Jungbluth, N. C. Voermans, E.-J. Kamsteeg, *RYR1*-related myopathies: A wide spectrum of phenotypes throughout life. *Eur. J. Neurol.* **22**, 1094–1112 (2015).
23. H. Zhou, S. Lillis, R. E. Loy, F. Ghassemi, M. R. Rose, F. Norwood, K. Mills, S. Al-Sarraj, R. J. M. Lane, L. Feng, E. Matthews, C. A. Sewry, S. Abbs, S. Buk, M. Hanna, S. Treves, R. T. Dirksen, G. Meissner, F. Muntoni, H. Jungbluth, Multi-minicore disease and atypical periodic paralysis associated with novel mutations in the skeletal muscle ryanodine receptor (*RYR1*) gene. *Neuromuscul. Disord.* **20**, 166–173 (2010).
24. Y. Liu, N. L. Jennings, A. M. Dart, X.-J. Du, Standardizing a simpler, more sensitive and accurate tail bleeding assay in mice. *World J. Exp. Med.* **2**, 30–36 (2012).
25. M. Vukcevic, F. Zorzato, S. Keck, D. A. Tsakiris, J. Keiser, R. M. Maizels, S. Treves, Gain of function in the immune system caused by a ryanodine receptor 1 mutation. *J. Cell Sci.* **126**, 3485–3492 (2013).
26. C. J. Hartley, A. K. Reddy, S. Mandala, M. L. Entman, L. H. Michael, G. E. Taffet, Doppler velocity measurements from large and small arteries of mice. *Am. J. Physiol. Heart Circ. Physiol.* **301**, H269–H278 (2011).
27. J. C. Sullivan, B. Wang, E. I. Boesen, G. D'Angelo, J. S. Pollock, D. M. Pollock, Novel use of ultrasound to examine regional blood flow in the mouse kidney. *Am. J. Physiol. Renal Physiol.* **297**, F228–F235 (2009).
28. P. J. Pritchard, J. C. Leylegian, R. Bhaskaran, *Fox and McDonald's Introduction to Fluid Mechanics* (John Wiley & Sons, New York, ed. 8, 2015).
29. D. Paulin, Z. Li, Desmin: A major intermediate filament protein essential for the structural integrity and function of muscle. *Exp. Cell Res.* **301**, 1–7 (2004).
30. M. F. Navedo, G. C. Amberg, R. E. Westenbroeck, M. J. Sinnegger-Brauns, W. A. Catterall, J. Striessnig, L. F. Santana, Cav1.3 channels produce persistent calcium sparklets, but $Ca_v1.2$ channels are responsible for sparklets in mouse arterial smooth muscle. *Am. J. Physiol. Heart Circ. Physiol.* **293**, H1359–H1370 (2007).
31. M. Gollasch, H. Haase, C. Ried, C. Lindschau, I. Morano, F. C. Luft, H. L. Haller, L-type calcium channel expression depends on the differentiated state of vascular smooth muscle cells. *FASEB J.* **12**, 593–601 (1998).
32. X.-R. Yang, M.-J. Lin, K.-P. Yip, L. H. Jeyakumar, S. Fleischer, G. P. H. Leung, J. S. K. Sham, Multiple ryanodine receptor subtypes and heterogeneous ryanodine receptor-gated Ca^{2+} stores in pulmonary arterial smooth muscle cells. *Am. J. Physiol. Lung Cell. Mol. Physiol.* **289**, L338–L348 (2005).
33. R. E. Lesh, G. F. Nixon, S. Fleischer, J. A. Airey, A. P. Sompliy, A. V. Somlyo, Localization of ryanodine receptors in smooth muscle. *Circ. Res.* **82**, 175–185 (1998).
34. L. M. Lifshitz, J. D. Carmichael, F. A. Lai, V. Sorrentino, K. Bellvé, K. E. Fogarty, R. ZhuGe, Spatial organization of RYRs and BK channels underlying the activation of STOCs by Ca^{2+} sparks in airway myocytes. *J. Gen. Physiol.* **138**, 195–209 (2011).
35. J. H. Clark, N. P. Kinnear, S. Kalujnaia, G. Cramb, S. Fleischer, L. H. Jeyakumar, F. Wuytack, A. M. Evans, Identification of functionally segregated sarcoplasmic reticulum calcium stores in pulmonary arterial smooth muscle cells. *J. Biol. Chem.* **285**, 13542–13549 (2010).
36. P. T. Nowiki, S. Flavahan, H. Hassanain, S. Mitra, S. Holland, P. J. Goldschmidt-Clemons, N. A. Flavahan, Redox signalling of the arteriolar myogenic response. *Circ. Res.* **89**, 114–116 (2001).
37. S. Treves, A. A. Anderson, S. Ducreux, A. Divet, C. Bleunven, C. Grasso, S. Paesante, F. Zorzato, Ryanodine receptor 1 mutation, dysregulation of calcium homeostasis and neuromuscular disorders. *Neuromuscul. Disord.* **15**, 577–587 (2005).
38. R. Robinson, D. Carpenter, M.-A. Shaw, J. Halsall, P. Hopkins, Mutations in *RYR1* in malignant hyperthermia and central core disease. *Hum. Mutat.* **27**, 977–989 (2006).
39. A. D. Lyfenko, S. A. Goonasekera, R. T. Dirksen, Dynamic alterations in myoplasmic Ca^{2+} in malignant hyperthermia and central core disease. *Biochem. Biophys. Res. Commun.* **322**, 1256–1266 (2004).
40. T. Girard, D. Cavagna, E. Padovan, G. Spagnoli, A. Urwyler, F. Zorzato, S. Treves, B-lymphocytes from malignant hyperthermia-susceptible patients have an increased sensitivity to skeletal muscle ryanodine receptor activators. *J. Biol. Chem.* **276**, 48077–48082 (2001).
41. S. Fleischer, M. Inui, Biochemistry and biophysics of excitation–contraction coupling. *Annu. Rev. Biophys. Chem.* **18**, 333–364 (1989).
42. L. Xu, Y. Wang, N. Yamaguchi, D. A. Pasek, G. Meissner, Single channel properties of heterotetrameric mutant RyR1 ion channels linked to core myopathies. *J. Biol. Chem.* **283**, 6321–6329 (2008).
43. S. C. Jackson, L. Odiaman, R. T. Card, J. G. van der Bom, M.-C. Poon, Suspected collagen disorders in the bleeding disorder clinic: A case-control study. *Haemophilia* **19**, 246–250 (2013).
44. G. Wiegand, M. Hofbeck, M. Zenker, U. Budde, R. Rauch, Bleeding diathesis in Noonan syndrome: Is acquired von Willebrand syndrome the clue? *Thromb. Res.* **130**, e251–e254 (2012).
45. G. Krishnamoorthy, S. K. Sonkusare, T. J. Heppner, M. T. Nelson, Opposing roles of smooth muscle BK channels and ryanodine receptors in the regulation of nerve-evoked constriction of mesenteric resistance arteries. *Am. J. Physiol. Heart Circ. Physiol.* **306**, H981–H988 (2014).
46. H. Cheng, W. J. Lederer, Calcium sparks. *Physiol. Rev.* **88**, 1491–1545 (2008).
47. Y. Li, R. A. Lorca, X. Ma, A. Rhodes, S. K. England, BK channels regulate myometrial contraction by modulating nuclear translocation of NF- κ B. *Endocrinology* **155**, 3112–3122 (2014).
48. C. R. Rosenfeld, T. Roy, Large conductance Ca^{2+} -activated and voltage-activated K⁺ channels contribute to the rise and maintenance of estrogen-induced uterine vasodilation and maintenance of blood pressure. *Endocrinology* **153**, 6012–6020 (2012).
49. N. Fritz, J.-L. Morel, L. H. Jeyakumar, S. Fleischer, P. D. Allen, J. Mironneau, N. Macrez, RyR1-specific requirement for depolarization-induced Ca^{2+} sparks in urinary bladder smooth muscle. *J. Cell Sci.* **120**, 3784–3791 (2007).
50. M. Bowman, G. Mundell, J. Grabell, W. M. Hopman, D. Rapson, D. Lillicrap, P. James, Generation and validation of the condensed MCMMDM-1VVD bleeding questionnaire for von Willebrand disease. *J. Thromb. Haemost.* **6**, 2062–2066 (2008).
51. S. Tao, D. Yamazaki, S. Komazaki, C. Zhao, T. Iida, S. Kakizawa, Y. Imaizumi, H. Takeshima, Facilitated hyperpolarization signaling in vascular smooth muscle-overexpressing TRIC-A channels. *J. Biol. Chem.* **288**, 15581–15589 (2013).
52. M. Sekulic-Jablanovic, A. Palmowski-Wolfe, F. Zorzato, S. Treves, Characterization of excitation–contraction coupling components in human extraocular muscles. *Biochem. J.* **466**, 29–36 (2015).
53. J. Schindelin, I. Arganda-Carreras, E. Frise, V. Kaynig, M. Longair, T. Pietzsch, S. Preiblich, C. Rueden, S. Saalfeld, B. Schmid, J. Y. Tinevez, D. J. White, V. Hartenstein, K. Eliceiri, P. Tomancak, A. Cardona, Fiji: An open-source platform for biological-image analysis. *Nat. Methods* **9**, 676–682 (2012).
54. E. Picht, A. V. Zima, L. A. Blatter, D. M. Bers, SparkMaster: Automated calcium spark analysis with ImageJ. *Am. J. Physiol. Cell Physiol.* **293**, C1073–C1081 (2007).
55. H. Zhou, O. Rokach, L. Feng, I. Munteanu, K. Mamchaoui, J. M. Wilmshurst, C. Sewry, A. Y. Manzur, K. Pillay, V. Mouly, M. Duchen, H. Jungbluth, S. Treves, F. Muntoni, RyR1 deficiency in congenital myopathies disrupts excitation–contraction coupling. *Hum. Mutat.* **34**, 986–996 (2013).
56. V. Dell'Asta, R. Gatti, G. Orlandini, P. A. Rossi, B. M. Rotoli, R. Sala, O. Bussolati, G. C. Gazzola, Membrane potential changes visualized in complete growth media through confocal laser scanning microscopy of bis-oxonol-loaded cells. *Exp. Cell Res.* **231**, 260–267 (1997).

Acknowledgments: We thank A.-S. Monnet for technical support and our patients for their participation. We thank S. Hamilton (Baylor College of Medicine, Houston, TX) for the heterozygous *RYR1*_{V522S} knock-in mice. **Funding:** This work was supported by a grant from the Swiss NSF (SNF No. 31003A-146198). The support of the Department of Anesthesia Basel University Hospital is gratefully acknowledged. **Author contributions:** R.J.L. designed and performed the experiments and analyzed the results with guidance from F.Z. and S.T.; M.V. performed the first bleeding experiments in the mice and helped measure membrane potential. M.S.-J. performed the qPCR experiments. L.X. performed the pulsed wave Doppler experiments under the supervision of M.B. H.Z. investigated RyR1 expression in platelets. S.B., M.S., E.C., H.J., J.A., N.V., F.M., A.R., S.M., and E.W. were involved in patient selection, identification of mutations, phenotypic and genetic characterization, and characterization of bleeding properties. F.Z. and S.T. designed the experiments on the mouse model, oversaw the project, and wrote the paper together with H.J.; H.J. made the initial observation of bleeding abnormalities in the patients and conceived the idea for this project together with F.Z. and S.T. **Competing interests:** The authors declare that they have no competing interests.

Submitted 2 December 2015

Accepted 9 June 2016

Final Publication 5 July 2016

10.1126/scisignal.aad9813

Citation: R. J. Lopez, S. Byrne, M. Vukcevic, M. Sekulic-Jablanovic, L. Xu, M. Brink, J. Alameli, N. Voermans, M. Snoeck, E. Clement, F. Muntoni, H. Zhou, A. Radunovic, S. Mohammed, E. Wraige, F. Zorzato, S. Treves, H. Jungbluth, An *RYR1* mutation associated with malignant hyperthermia is also associated with bleeding abnormalities. *Sci. Signal.* **9**, ra68 (2016).

An *RYR1* mutation associated with malignant hyperthermia is also associated with bleeding abnormalities

Rubén J. Lopez, Susan Byrne, Mirko Vukcevic, Marijana Sekulic-Jablanovic, Lifen Xu, Marijke Brink, Jay Alamelu, Nicol Voermans, Marc Snoeck, Emma Clement, Francesco Muntoni, Haiyan Zhou, Aleksandar Radunovic, Shehla Mohammed, Elizabeth Wraige, Francesco Zorzato, Susan Treves and Heinz Jungbluth (July 5, 2016)

Science Signaling **9** (435), ra68. [doi: 10.1126/scisignal.aad9813]

The following resources related to this article are available online at <http://stke.sciencemag.org>.
This information is current as of July 6, 2016.

- | | |
|-------------------------------|--|
| Article Tools | Visit the online version of this article to access the personalization and article tools: http://stke.sciencemag.org/content/9/435/ra68 |
| Supplemental Materials | " <i>Supplementary Materials</i> " http://stke.sciencemag.org/content/suppl/2016/06/30/9.435.ra68.DC1 |
| Related Content | The editors suggest related resources on <i>Science's</i> sites: http://stke.sciencemag.org/content/sigtrans/7/317/ra27.full http://stke.sciencemag.org/content/sigtrans/7/327/ra49.full http://stke.sciencemag.org/content/sigtrans/8/358/ra2.full http://science.sciencemag.org/content/sci/333/6048/1440.full http://science.sciencemag.org/content/sci/253/5018/448.full.pdf http://stm.sciencemag.org/content/scitransmed/4/164/164ra160.full |
| References | This article cites 54 articles, 22 of which you can access for free at: http://stke.sciencemag.org/content/9/435/ra68#BIBL |
| Permissions | Obtain information about reproducing this article: http://www.sciencemag.org/about/permissions.dtl |